Article

pubs.acs.org/Biomac

Mechanistic Design of Chemically Diverse Polymers with Applications in Oral Drug Delivery

Laura I. Mosquera-Giraldo,[†] Carlos H. Borca,[‡] Xiangtao Meng,[§] Kevin J. Edgar,[§] Lyudmila V. Slipchenko,[‡] and Lynne S. Taylor*[,†]

[†]Department of Industrial and Physical Pharmacy, College of Pharmacy, Purdue University, West Lafayette, Indiana, United States

[‡]Department of Chemistry, College of Science, Purdue University, West Lafayette, Indiana, United States

[§]Department of Sustainable Biomaterials, College of Natural Resources and Environment, Virginia Tech, Blacksburg, Virginia, United States

Supporting Information

ABSTRACT: Polymers play a key role in stabilizing amorphous drug formulations, a recent strategy employed to improve solubility and bioavailability of drugs delivered orally. However, the molecular mechanism of stabilization is unclear, therefore, the rational design of new crystallization-inhibiting excipients remains a substantial challenge. This article presents a combined experimental and computational approach to elucidate the molecular features that improve the effectiveness of cellulose polymers as solution crystallization inhibitors, a crucial first step toward their rational design. Polymers with chemically diverse substituents including carboxylic acids, esters, ethers, alcohols, amides, amines, and sulfides were synthesized. Measurements of nucleation induction times of the model drug, telaprevir, show that the only effective polymers contained carboxylate groups in combination with an optimal hydrocarbon chain length. Computational results indicate that polymer conformation as well as solvation free energy are important determinants of effectiveness at inhibiting crystallization and show that simulations are a promising predictive tool in the screening of polymers. This study suggests that polymers need to have an adequate hydrophilicity to promote solvation in an aqueous environment, and sufficient hydrophobic regions to drive interactions with the drug. Particularly, the right balance between key substituent groups and lengths of hydrocarbon side chains is needed to create effective materials.

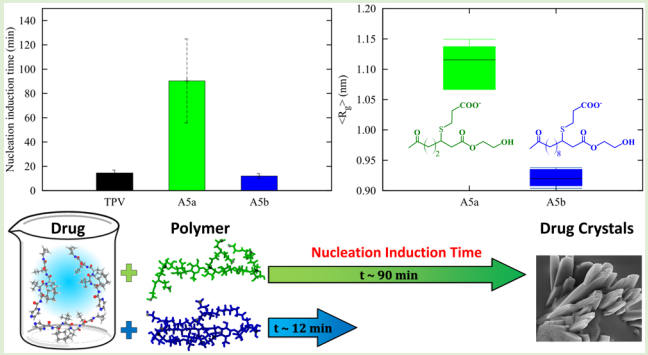

INTRODUCTION

The increasing number of new drugs with low aqueous solubility poses a challenge for their oral delivery, since a bioactive substance must be dissolved to have a therapeutic effect.[1−3] This has bolstered the interest in amorphous materials, that is, solids that lack long-range, three-dimensional order, as a strategy to improve drug solubility and bioavailability.[1−4] However, the amorphous form of a drug is thermodynamically unstable due to its high free energy, and it will eventually crystallize, decreasing its solubility.[5] Polymers can be employed to stabilize the amorphous state of a drug and prolong the duration of the higher drug concentrations achieved in an aqueous medium following dissolution.[6] In essence, the polymer and the drug are intimately mixed and the resultant polymer−drug molecular blend is typically referred to as an amorphous solid dispersion (ASD).[3]

Perhaps the most important question when designing an ASD is which polymer is best suited for formulation with a specific drug? Unfortunately, polymer selection is still largely empirical,[7] and the majority of marketed ASDs are formulated with the same limited set of commercially available polymers. The lack of chemical diversity of polymers used in these formulations, combined with the increasing interest in ASDs, has stimulated the creation of materials with optimized properties for crystallization inhibition of drugs.[8−12] Nonetheless, the understanding of how chemical modifications to the polymer impact its effectiveness is incomplete, posing an obstacle for the rational selection of existing polymers and the design of new ones.

The complexity of commercial cellulose polymers impedes mechanistic studies to identify the chemical groups that most improve polymer effectiveness. As a result, diverse analogs of hydroxypropyl methyl cellulose (HPMC) and acetate succinate (HPMCAS) have been synthesized to determine the effects of each substituent.[9,11,13] Ting et al. demonstrated the importance of succinoyl, as well as alcohol substituents, in the performance of HPMCAS analogs;[9,11] and Yin and Hillmyer obtained effective polymers when HPMC esters were substituted with

Received: July 28, 2016
Revised: September 21, 2016
Published: September 22, 2016

DOI: 10.1021/acs.biomac.6b01156
Biomacromolecules 2016, 17, 3659−3671

succinoyl and thioethers attached to cyclohexyl and benzene groups.[13]

In recent years, a number of cellulose derivatives has been produced, taking advantage of innovative synthetic approaches.[10,14−20] The ability of these polymers to inhibit the crystallization of poorly water-soluble drugs has been evaluated in turn.[8,21] Ilevbare et al. reported nucleation induction times for three model drugs in the presence of newly synthesized and commercial polymers.[8] Some of these new polymers were equally or more effective than their commercial counterparts, an improvement explained by a good match between the solubility parameter of drug and polymer.[8] In addition, the polymers were effective at reducing crystal growth,[22] due to the favorable adsorption of the polymer on the crystal surface, as corroborated by recent studies employing atomic force microscopy (AFM).[23,24] It was further proposed that crystal growth inhibition can be related to the conformation of the polymer on the surface.[23,24]

Although several cellulose based polymers have been studied previously in terms of their ability to delay nucleation, they were chemically similar: cellulose ester substituents with various hydrocarbon lengths and a carboxylic acid termination. Recent development in innovative cellulose modification methods by Meng et al., including hydroboration-oxidation,[17] olefin cross-metathesis,[14−16] and a double modification strategy by post cross-metathesis thiol-Michael addition,[20] provide an opportunity to obtain a variety of functionalized cellulose derivatives. Investigating polymers with greater chemical diversity enables deeper fundamental insight into structure−property−activity relationships, which in turn helps inform the design of new materials, and will ultimately lead to rational, rather than empirical, polymer selection.

There are significant limitations in the current approach to design new, effective polymers. Certain properties of existing polymers have been recognized to be important. For example, one approach has been optimizing solubility parameter.[8,19,25] Tuning the glass-transition temperature has been another approach. Carboxylic and bulky groups have been identified as features impacting polymer performance.[8] However, when exploring polymers with significantly different chemical or structural modifications, there is no clear correlation between these properties and their effectiveness. Thus, determination of the effectiveness of newly synthesized polymers is an expensive trial and error process. A deeper understanding of the underlying chemistry of these systems is required to overcome those limitations.

Computational techniques, such as molecular dynamics (MD) simulations and quantum chemical calculations offer an alternative perspective to explore the chemistry of these polymers in atomistic detail. There is a small number of modeling studies related to ASDs, despite its importance in the area of oral drug delivery. Anwar et al. performed Lennard-Jones MD simulations showing that the effectiveness of an additive at inhibiting nucleation is dependent on a balance between the degree of self-interaction of the additive and on the additive-solute affinity.[26] Jha et al. performed MD simulations with phenytoin and HPMC with and without acetate and succinate groups.[27] They showed that an increase in polymer concentration causes a decrease in the probability of crystallization, possibly due to a decrease in the molecular mobility.[27] Gao and Olsen simulated a tolzamide crystal in the presence of two types of oligomers, and reported that van der Waals and hydrophobic interactions between polymer and crystal influence crystal growth inhibition.[28] There are also reports of simulations that calculate monomer−drug binding energies and drug encapsulation in polymeric carriers.[29−32]

Herein we present a combined experimental and computational approach to illuminate, from a molecular level, factors that may impact polymer effectiveness. We explore how chemically diverse substituents influence the effectiveness of cellulose polymers as crystallization inhibitors. The chemical substituents include carboxylic acids, esters, ethers, alcohols, amides, amines, and sulfides. Telaprevir, a protease inhibitor used in the treatment of hepatitis C, and formulated as an ASD due to its poor aqueous solubility, is used as the model drug compound.[33] The experimental work provides information about which chemical modifications generate polymers with the best crystallization inhibitory properties for this compound. Computational modeling is used to rationalize the ways in which changes in the chemical structure influence intramolecular interactions in the polymer, that in turn explain variations in crystallization inhibition effectiveness. Our contribution constitutes a generalizable example of how computational simulations, aimed at guiding polymer synthesis, permit the design of new materials and optimization of future pharmaceutical formulations.

MATERIALS AND METHODS

Materials. Telaprevir was purchased from Attix Pharmaceuticals (Toronto, Ontario, Canada). The commercially available polymers (Table 1) were obtained from various suppliers: HPMC 606 grade and HPMCAS-MF (Shin-Etsu Chemical Co., Ltd., Tokyo, Japan); PVP K29/32, PAA, CAPh, and pectin from citrus peel (Sigma-Aldrich Co St. Louis MO); Eudragit L100 (Degussa, Rohm GmbH & Co. KG, Germany); and PVP-VA K28 (BASF, Germany). The new cellulose-based polymers (Figure 1 and Table S1 in the Supporting Information) were synthesized as described in the next subsection.

Table 1. Abbreviations of Commercially Available Polymers

polymer	abbreviation
poly(vinylpyrrolidone) (K 29/32)	PVP
polyacrylic acid	PAA
poly(vinylpirrolidone vinyl acetate) (K 28)	PVPVA
cellulose acetate phthalate	CAPhth
hydroxypropyl methyl cellulose	HPMC
hydroxypropyl methyl cellulose acetate succinate (AS-MF)	HPMCAS
eudragit L100	EUD L100

The aqueous media used in all experiments was 100 mM sodium phosphate buffer pH 6.8 prepared by adding 6.956 g sodium phosphate dibasic anhydrous and 7.0375 g monosodium phosphate monohydrate in 1 L of DI water.

Polymer Synthesis. The newly synthesized polymers are summarized in Table S1 in the Supporting Information and their chemical structures are shown in Figure 1. In most cases their syntheses have been previously described by us, and the original references are given below. These polymers were classified depending on the synthesis method employed.

For the synthesis of polymers **1−6** (Table S1), monobenzyl adipoyl/suberoyl/sebacoyl chlorides were synthesized from adipic/suberic/sebacic acids, respectively.[10] The afforded acid chloride was then employed in esterification reaction with a commercial cellulose ester, for example, cellulose acetate, to give a benzyl cellulose ester. The final cellulose ω-carboxyalkanoate was afforded by hydrogenolysis of the benzyl protecting group using $Pd(OH)_2/C$ as a catalyst in a H_2 atmosphere.[10]

Polymers **7−18** were prepared as previously described.[14−17,34] Commercially available cellulose esters (cellulose acetate CA-320S,

DOI: 10.1021/acs.biomac.6b01156
Biomacromolecules 2016, 17, 3659−3671

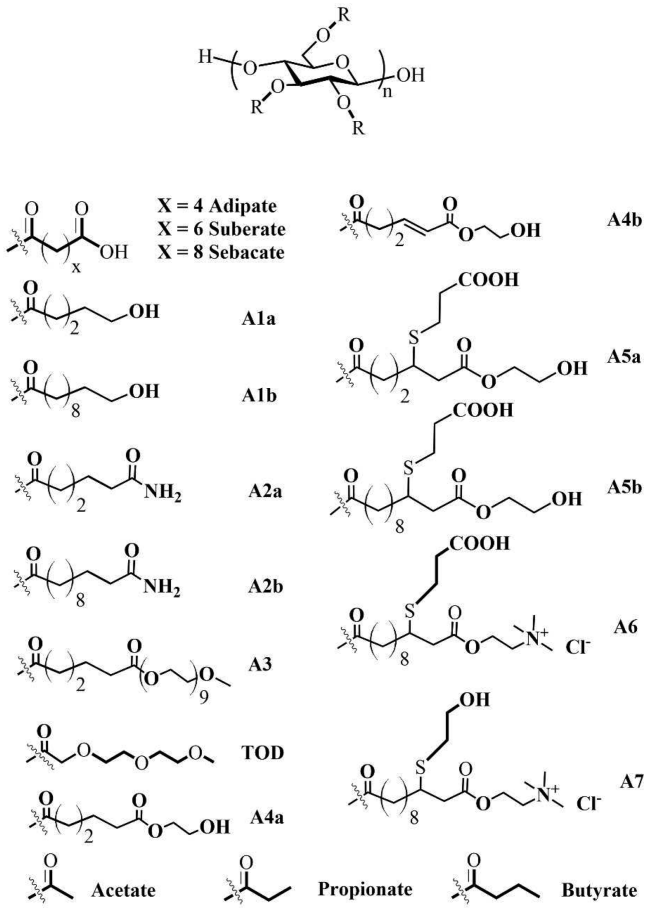

Figure 1. Molecular structures of synthesized cellulose polymers. Substituent R can be H or the moieties illustrated below the polymer structure.

cellulose acetate butyrate CAB-553−0.4, and cellulose acetate propionate CAP-504−0.2) were esterified with two terminally olefinic acid chlorides, that is, pent-4-enoyl chloride or undec-10-enoyl chloride, to be used as the starting materials for olefin cross-metathesis (CM). Three reaction pathways were then sorted for the synthesis of three groups of polymers.

Reaction Pathway 1. For polymers **7** and **11−14**, CM of the starting materials with different partners (acrylic acid, 2-hydroxyethyl acrylate, poly(ethylene glycol) methyl ether acrylate, and acrylamide)[14−16] was performed to give various functionalized cellulose esters. A subsequent hydrogenation step using either H_2−Pd/C[14] or *p*-toluenesulfonyl hydrazide[16] was performed to eliminate the α,β-unsaturation and give stable products.

Reaction Pathway 2. For polymers **15−18**, CM of the starting materials with partners (2-hydroxyethyl acrylate and [2-(acryloyloxy)-ethyl]trimethylammonium chloride) was first conducted. Instead of eliminating the α,β-unsaturation by hydrogenation, hydrothiolation (the addition of a thiol across a double bond) was performed by thiol-Michael addition reaction between 2-mercaptoethanol or 3-mercaptopropoinic acid and the α,β-unsaturation on the polymer side chain.[20] Using this double modification method, the cellulosic side chain can bear two types of functional groups. Although CM reaction has proven powerful and gave mostly complete conversion to various CM substrates, this was not the case when reacting short chain terminal olefin (CA-Pen079) with [2-(acryloyloxy)ethyl]trimethylammonium chloride to synthesize CA-Pen079-TMA. This is probably due to repulsion between trimethylammonium cationic moieties that are held in close proximity by the short ethers to the cellulose backbone. Long side-chain derivatives such as CA-Un067 did not display such an issue since the longer chains permit larger spacing between charges. Thus, CA-Un067-TMA and the related derivatives were synthesized successfully. Definitions of these polymer abbreviations (reported in previous articles) relative to the ones shown in Table S2 can be found in the Supporting Information.

Reaction Pathway 3. For polymers **8−10**, the side chain terminal olefins on the starting materials were transformed quantitatively to hydroxyl functionality by hydroboration-oxidation reaction.[17]

Solubility Parameter (SP) Calculations. SP values were calculated by the Fedor's method and following a procedure similar to that of Babcock et al.[25,35] It considers the energy of vaporization, molar volume and the degree of substitution for the diverse substituents. The SP calculation procedure is described in detail in the Supporting Information in the paper by Dong et al.[19]

Nucleation-Induction Time Experiments. The newly synthesized cellulose polymers were predissolved by adding a small amount of organic solvent (Table S1 in the Supporting Information), followed by sonication until complete dissolution was achieved. Then, sodium phosphate buffer pH 6.8 100 mM was added and the solution was further sonicated. Polymer solutions were visually inspected to verify that the polymers were soluble at the concentration used (5 and/or 50 μg/mL). Commercially available polymers were directly dissolved in buffer.

The experimental nucleation time (T_{ind}) is defined as the sum of the time for critical nucleus formation (T_n) and for growth to a detectable size (T_{growth}) eq 1.

$$T_{ind} = T_n + T_{growth} \quad (1)$$

It has been previously reported that when telaprevir concentration in solution exceeds ~90−100 μg/mL a drug-rich phase is created, which consists of spherical aggregates with sizes in the range of 200−400 nm.[36] This second phase is glassy in nature due to the high temperature glass transition of telaprevir. Consequently, the process of phase separation which occurs when the binodal concentration is exceeded is termed glass−liquid phase separation (GLPS).[36,37] Because the presence of a second phase is likely to impact nucleation kinetics, by providing interfaces for heterogeneous nucleation, it is important to evaluate the effectiveness of polymers as nucleation inhibitors at supersaturations below and above where GLPS occurs, to compare and contrast crystallization in a homogeneous solution (molecularly dissolved drug) and a two-phase solution (molecularly dissolved drug and drug-rich particles).

Supersaturated solutions were prepared by adding 80 or 150 μg/mL of a telaprevir (TPV) methanolic stock solution (7 mg/mL) to 47 mL phosphate buffer (pH 6.8, 100 mM) held at 37 °C using a 50 mL jacketed flask coupled to a water bath, with magnetic stirring at 300 rpm.

The crystallization induction time from unseeded samples was measured using an SI Photonics UV/vis spectrometer (Tucson, Arizona) coupled to a fiber optic probe (path lengths 5 and 10 mm). Measurements were recorded every minute at two wavelengths: the maximum UV absorbance wavelength of TPV (270 nm) and a nonabsorbing wavelength (370 nm) to account for fluctuations in scattering caused by the existence of a second phase. The difference in absorbance between the two wavelengths was converted to concentration by using a standard curve with good linearity ($R^2 > 0.999$).

For experiments performed at 80 μg/mL TPV, which is below the GLPS concentration for telaprevir, the increase in the nonabsorbing wavelength (370 nm) and the decrease in the absorbing wavelength (270 nm) were taken as the induction times. For experiments performed at 150 μg/mL TPV concentration, the nonabsorbing wavelength was not used since scattering centers are already present in the solution; hence, induction times were inferred from changes in the signal at 270 nm.

Scanning Electron Microscopy (SEM). Liquid samples were extracted from the induction time experiments, added to a coverslip and placed into the vacuum oven to remove any remaining liquid. Next, the samples were sputtered with platinum for 120 s and imaged with a FEI NOVA nanoSEM field emission SEM (Hillsboro, Oregon), using an Everhart−Thornley detector (ETD) and through-the-lens detector (TLD). The parameters were 5 kV accelerating voltage, ~5−6 mm working distance, beam spot size of 3, 30 μm aperture, and magnifications in the 5000−30000× range.

DOI: 10.1021/acs.biomac.6b01156
Biomacromolecules 2016, 17, 3659−3671

Computational Simulations. *Quantum Chemical Calculations.* To provide insight into the effect of substituents on the chemical properties of the cellulose-based polymers, Density Functional Theory (DFT) calculations were performed. The hybrid Perdew–Burke–Ernzerhof exchange-correlation density functional (PBE0)[38,39] with Pople's 6-31+G* basis set were employed in all cases. All the calculations were performed using the Polarizable Continuum Model (PCM) with the dielectric constant for water (78.39), to account for solvent effects.[40,41] Chemical structures of average repeat units (termed herein "monomers") of the newly synthesized polymers were drawn in the visualization software IQmol 2.5.[42] The monomer chain terminals were capped with methyl groups, to diminish any border effects. Substitutions were applied on the R_6 group, which is the most stereoaccessible location in the monomers. The other R groups where substituted by hydrogen atoms. Models including carboxylic acid groups were simulated in their anionic form, to resemble experimental pH conditions. In the cellulose polymer with the adipate substitution, the carboxylic acid group was simulated in both protonated and ionic forms.

A conformational search for each monomer was performed with CHARMM force field in HyperChem 8.0.3.[43] In each case, specific torsions were chosen, and a random walk method was used to vary these torsions, with an acceptance criterion of maximum 6 kcal/mol above best and a total of 1000 optimization cycles. After each conformational search, the structure with lower energy was selected for the following steps. The initial telaprevir structure was extracted from a crystalline structure report, and this conformation was then optimized.[44]

Using the Q-Chem 4.3[45] computational chemistry package, the structures were optimized using tight convergence criteria for the Self-Consistent Field Procedure. Then, single-point energy calculations were executed over the optimized structures, using the same level of theory and basis set. The outputs of the latter calculations were employed to produce plots of the Molecular Electrostatic Potential mapped over the electronic density, based on the Gasteiger-Marsili empirical atomic partial charges, using IQmol 2.5.[42] The free energy of solvation for each monomer is reported as well.

Molecular Dynamics Simulations. To provide insight into the dynamics of oligomers, atomistic MD simulations were carried out in GROMACS 5.0,[46,47] using the CHARMM force field.[48,49] The systems were prepared in eight steps.

(1) First, chemical structures of the oligomers were drawn in HyperChem 8.0.3.[43] Each oligomer included seven monomers, and three of the monomers were substituted, with the same side chain, on the R_6 group. A general schematic is shown in Figure 8.

(2) An energy minimization was performed on these structures, with the Polak-Ribière (conjugate-gradient) algorithm, using a maximum of 3×10^5 steps, and a root-mean-square (RMS) gradient of 1.0×10^{-2} kcal Å^{-1} mol^{-1} as convergence conditions.

(3) These structures were submitted to the online topology building tool SwissParam,[50] used to obtain topology files in GROMACS format. Then, the oligomers were solvated using the extended simple point charge (SPC/E) water model. Three Na^+ ions were used as mobile counterions for oligomers with carboxylate groups. The largest oligomer included more than 300 atoms. When solvated, the systems included ~21000 water molecules in cubic boxes with edges of up to 8.6 nm.

The five subsequent steps, four equilibration stages and the production run, were executed using GROMACS 5.0. The velocity-Verlet algorithm was used as integrator. Periodic Boundary Conditions were employed with the Verlet cutoff scheme for neighbor searching. Short-range electrostatic interactions were modeled with a cutoff of 1 nm, and the Particle Mesh Ewald (PME)[51] method was used for long-range electrostatics. van der Waals interactions were calculated until a cutoff of 1 nm.

(4) First, a microcanonical ensemble (NVE) equilibration was run in GROMCAS for 50 ps (0.5 fs/step) to relax the system and minimize any close contacts introduced in the solvation process.

(5) Second, a canonical ensemble equilibration (NVT) was performed for 5 ns (1 fs/step) using the v-rescale thermostat, at a reference temperature of 310 K, with a coupling constant (tau-t) of 0.2 ps.

(6) Third, a fast isothermal–isobaric equilibration (NPT) was employed for 5 ns (1 fs/step) using the v-rescale thermostat, at a reference temperature of 310 K, with a coupling constant (tau-t) of 0.2 ps; and the Berendsen barostat at a reference pressure of 1 bar, with a coupling constant (tau-p) of 0.2 ps.

(7) Fourth, an isothermal–isobaric equilibration (NPT) was run for 5 ns (1 fs/step) using the Nosé–Hoover thermostat, at a reference temperature of 310 K, with a coupling constant (tau-t) of 0.2 ps; and the Martyna-Tuckerman-Tobias-Klein barostat at a reference pressure of 1 bar, with a coupling constant (tau-p) of 1.0 ps.

(8) Finally, the production run was performed for 40 ns (1 fs/step recording output every 5 fs) in the isothermal–isobaric (NPT) ensemble using the Nosé–Hoover thermostat, at a reference temperature of 310 K, with coupling constant (tau-t) of 0.2 ps; and the Martyna-Tuckerman-Tobias-Klein barostat at a reference pressure of 1 bar, with coupling constant (tau-p) of 1.0 ps.

The trajectories from the production run were examined. The radius of gyration (R_g), radial distribution functions (RDF), and solvent accessible surface (SAS) areas were analyzed for each type of oligomer.

R_g is a scalar metric that describes the structure and dimensions of a distribution of particles. For a system containing N particles, R_g is defined as

$$R_g^2 \equiv \frac{\sum_i^N m_i(\mathbf{r} - \mathbf{r}_{com})^2}{\sum_i^N m_i} \tag{2}$$

where m_i and $\mathbf{r}$ are the mass and position vector of the ith particle, respectively, and $\mathbf{r}_{com}$ is the position of the molecular center of mass.

If each of the atoms of a molecule is represented by a sphere of its corresponding van der Waals radius, the SAS is the outermost contour described by a 1.4 Å radius ball, which represents a water molecule, rolling over each of the atoms in the molecule. Then the total area is normalized by the number of atoms in each molecule.

The radial distribution function (RDF), $g_{\alpha\beta}(r)$, is a type of a pair correlation function that describes the orientation-normalized probability of finding a particle, of a given type, at a certain distance from a reference particle. For a system containing N_α particles of type α, and N_β particles of type β, the RDF is defined as

$$g_{\alpha\beta}(r) = \frac{1}{N_\alpha N_\beta} \sum_i^{N_\alpha} \sum_j^{N_\beta} \langle \delta(|\mathbf{r}_{ij}| - r) \rangle \tag{3}$$

where the angled brackets signify a time average, δ denotes the Dirac delta function, $|\mathbf{r}_{ij}|$ is the magnitude of the separation vector between particles i and j, and r represents the average distance between particles in an ideal gas distribution.

RESULTS

Influence of Polymer Structure on Nucleation-Induction Times. Supersaturated solutions of telaprevir crystallize rapidly in the absence of polymers. Therefore, addition of crystallization inhibitors is necessary to maintain supersaturation for biologically relevant timeframes. A diverse set of commercially available and new cellulose polymers synthesized for this purpose was therefore evaluated with the goal of determining which chemical and structural features are critical for crystallization inhibition.

The set of commercial polymers included pectin, PVP, PAA, PVPVA, HPMC, CAPhth, HPMCAS, and EUD L100 with induction time results shown in Figure 2a. The polymers are

DOI: 10.1021/acs.biomac.6b01156
Biomacromolecules 2016, 17, 3659–3671

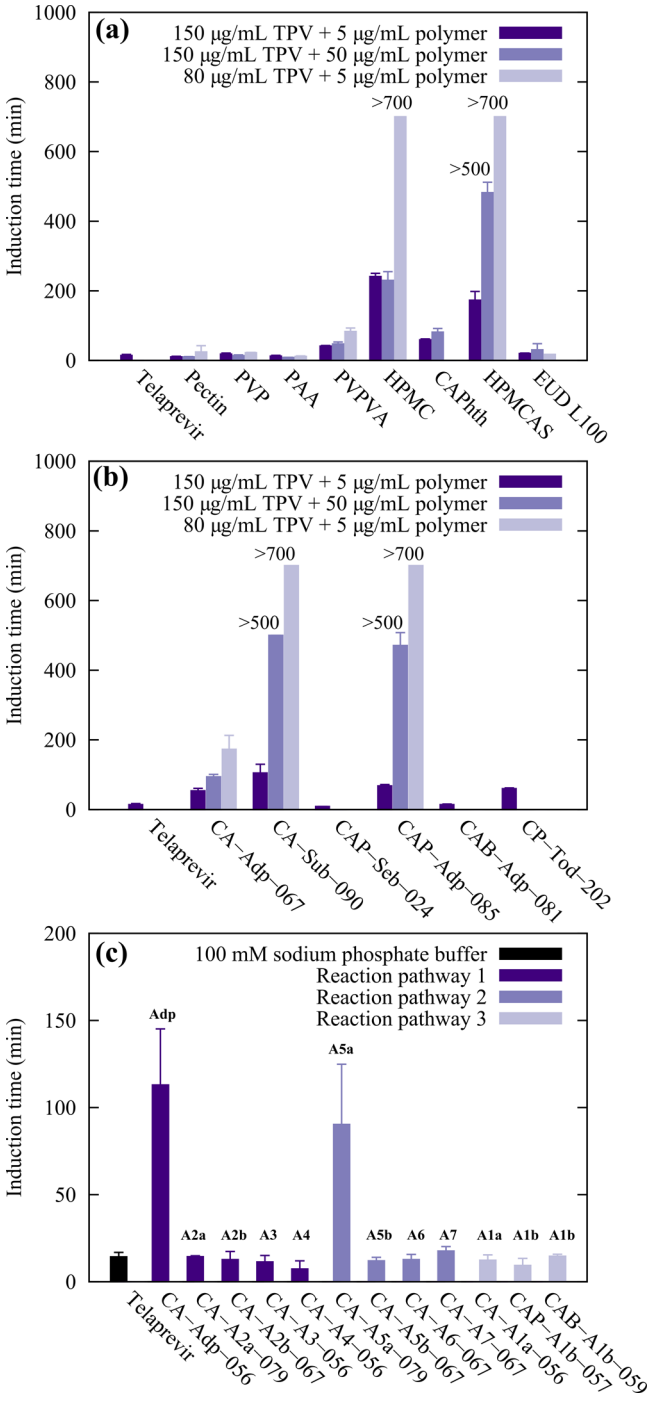

Figure 2. Induction time for telaprevir (TPV) in the presence of predissolved polymers (n = 3). (a) Commercially available polymers at 5 and 50 μg/mL concentrations with 150 or 80 μg/mL TPV, (b) cellulose ω-carboxyalkanoates polymers at 5 and 50 μg/mL concentrations with 150 or 80 μg/mL TPV, (c) polymers with chemically diverse substituents prepared by three different reaction pathways; 5 μg/mL polymer and 150 μg/mL drug were used. The substituent side chain abbreviation is indicated on the label above each bar.

ranked in order of decreasing solubility parameter (SP) from left to right, pectin with the highest SP and EUD L100 with the lowest SP.[24] When the initial telaprevir concentration was 80 μg/mL (homogeneous solution), HPMC and HPMCAS maintained the supersaturation for more than 700 min. Increasing the drug concentration to 150 μg/mL and thus creating a drug-rich amorphous phase,[36] led to reduced induction times relative to the comparable system with a lower TPV concentration. An increase in polymer concentration from 5 to 50 μg/mL resulted in longer induction times for HPMCAS. In contrast, increasing the HPMC concentration did not change the induction time relative to the lower concentration of this polymer. Therefore, in a maximally supersaturated TPV solution containing drug-rich amorphous particles, HPMCAS-MF was more effective than HPMC at 50 μg/mL.

The newly synthesized polymers were divided into two groups based on their structures. The first group comprises the cellulose ω-carboxyalkanoates (Figure 2b), which are cellulose esters containing substituents with various hydrocarbon lengths and a terminal carboxylic acid group. The second group encompasses polymers with chemically diverse functionalities including carboxylic acids, esters, ethers, alcohol, amides, amines and sulfides (Figure 2c).

In Figure 2b the cellulose ω-carboxyalkanoates are ordered from high to low SP, whereby CA-Adp-067 has the highest SP and CP-Tod-202 the lowest SP within the group. Results obtained with the cellulose ω-carboxyalkanoates suggest that optimal SP as well as the number of carboxylic acid groups were influential features of the most effective polymers. For example, CAP-Adp-085 and CA-Sub-090 have SP values in the 22.46−23.18 $MPa^{1/2}$ range, and a high degree of substitution (DS) of carboxylic acid substituents, 0.85 and 0.90, respectively. In contrast, CAP-Seb-024 is ineffective (SP = 23.04 $MPa^{1/2}$), which may be attributed to the low extent of groups with a carboxylic acid termination (0.24), and the correspondingly higher number of other groups such as butyrate and acetate. In other words, SP alone is not sufficient to predict polymer effectiveness.

Polymers with a broad range of chemical substituents (Figure 1) were evaluated next. The degree of substitution and molecular weight were maintained as constant as possible, with the aim of exploring the effect of changing a specific functional group. The polymers were further classified depending on their synthesis reaction pathway, as described in the methodology section. The olefin cross-metathesis chemistry used to synthesize many of these polymers is modular and thus well-suited to this approach, since it permits attachment of a variety of terminal functional groups to a single polysaccharide derivative under mild conditions, thus, holding other variables like degree of polymerization (DP), DS, and position of other substituents constant.[14−16,19,20] In this way the contribution of a single variable, the nature of the terminal functional group, can be evaluated in isolation.

The first subset of these polymers varies based on the terminal functional group, allowing for the evaluation of the impact of amide, ester, ether, alcohol, and carboxylic acid groups. From the induction times observed for these polymers (Figure 2c, in dark purple), it is clear that the only effective polymer, CA-Adp-056, possessed a terminal carboxylic acid group.

Next, polymers with structure similar to A4 but with an additional branch were synthesized, using metathesis followed by thiol-Michael addition (reaction pathway 2),[20] and then evaluated: (A5a and A5b, Figure 2c, in medium purple). These results suggest that the addition of a branch that includes a terminal carboxylic acid group can drastically improve polymer effectiveness (A5a substituent, CA-A5a-079 polymer). However, the length of the hydrocarbon chain has a major impact on induction times. The polymer with a two carbon chain length (A5a substituent, CA-A5a-079 polymer) was considerably more

DOI: 10.1021/acs.biomac.6b01156
Biomacromolecules 2016, 17, 3659−3671

effective than the equivalent polymer that contained an eight carbon chain (A5b substituent, CA-A5b-067 polymer).

Polymers A6 and A7 also present similar functionality to A4, but are terminated with a quaternary amine group instead of an alcohol. The main difference between A6 and A7 is the branch termination: carboxylic acid vs alcohol group. Neither of these polymers were effective at inhibiting crystallization, which may be attributed either to the trimethylammonium cationic functionality or to the long hydrocarbon chain. Unfortunately, it was impossible to synthesize short chain derivatives possessing trimethylammonium termination. The results with these polymers show that the presence of structural modifications such as branches and bulky groups on the cellulose backbone may improve the effectiveness of the polymers, but only when key functional groups are present.

Lastly, polymers with an alcohol termination were obtained using reaction pathway 3: A1a and A1b substituents. These polymers were ineffective at inhibiting nucleation.

We do not find any correlation between SP and effectiveness within this diverse set of chemical substituents, although this approach had worked to some extent for the more chemically homogeneous set of cellulose ω-carboxyalkanoates. While CA-A5a-079 and CA-A5b-067 have similar solubility parameters, one is effective whereas the other is not (Table S1). Therefore, the single, simple metric SP, is again insufficient to predict polymer performance at inhibiting the crystallization of poorly water-soluble compounds. Even though SP values are usually used as an estimation of hydrophobicity,[8,23] they are not a direct measure of this property, limiting their application.

It has been previously hypothesized that the role of the carboxylic acid group is to impart amphiphilicity in polymers used as crystallization inhibitors. In particular, when ionized, these groups allow interaction of hydrophobic polymer regions with the hydrophobic drug, and the interaction of ionized groups with the aqueous phase at the drug−water interface, thus, interfering with crystal nucleation and growth.[8] Figure 3 clearly shows that polymers with a terminal carboxylic acid are only effective when ionized.

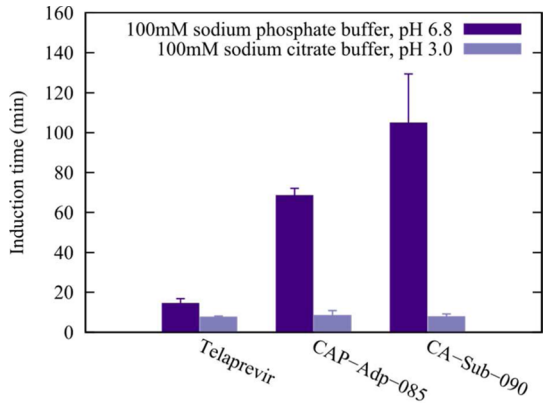

Figure 3. Induction time for telaprevir in the presence of predissolved polymers; 5 μg/mL polymer and 150 μg/mL drug (n = 3). The polymers were predissolved in buffer at two different pH values: pH 6.8 sodium phosphate buffer and pH 3.0 sodium citrate buffer. The figure shows that polymers with a carboxylic acid termination are effective when ionized, at pH 6.8, and ineffective when protonated, at pH 3.0.

Influence of Polymer Concentration in Nucleation-Induction Times and Crystal Sizes and Shapes. The impact of polymer concentration on nucleation induction times has not been widely studied and will likely depend on the polymer evaluated. Figure 4 shows the effect of polymer concentration on the induction times for telaprevir solutions. Although low, these are polymer concentrations that might be present in vivo following dissolution of an amorphous solid dispersion formulation. Notably, PVP is ineffective at any of the concentrations evaluated, while HPMCAS and CA-Sub-090 become more effective when the concentration is increased. In addition, at 5 μg/mL of polymer, HPMCAS is considerably more effective than CA-Sub-090, whereas at 50 μg/mL, they are equally effective.

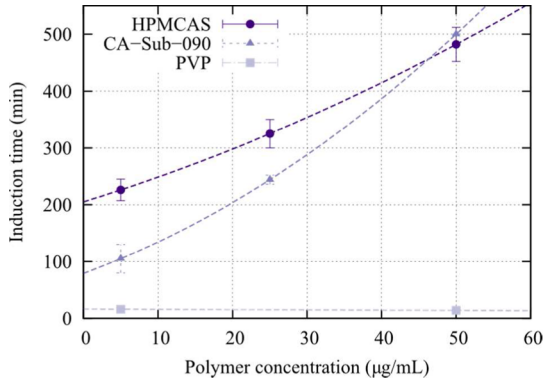

Figure 4. Induction time for telaprevir in the presence of predissolved polymers HPMCAS, CA-Sub-090, and PVP at different concentrations and 150 μg/mL drug (n = 3). The figure shows that the effectiveness of polymers at inhibiting crystallization does not follow a linear relationship in all cases.

These diverse polymers impact not only nucleation but also crystal growth, as reflected by the diverse resultant crystal shapes and sizes exhibited on Figure 5. The crystals obtained from HPMCAS-MF and CA-Sub-090 induction time experiments are much smaller than crystals formed in the absence of polymer or in the presence of PVP. From these preliminary observations, these two cellulose polymers may be effective crystal growth inhibitors, which will be evaluated in future work.

Computational Simulations. The experimental results clearly indicate the importance of carboxylate groups. Yet, several questions about structure−activity relationships remain unanswered: (1) why are two polymers with carboxylic acid terminations, but different carbon side chain lengths, such as A5a and A5b, so drastically different in their effectiveness as nucleation inhibitors; (2) why are polymers with a quaternary amine functional group, which is ionized at all pH values, ineffective inhibitors; and (3) how do different functional groups influence the polymer conformation and ability to interact with the drug? Consequently, a deeper understanding of structure−activity relationships is required and computational modeling was thus employed as a complementary tool capable of providing more detailed information about possible key interactions that could determine polymer effectiveness.

Quantum Chemical Calculations. The electronic structure of a molecule is a rich source of information about its fundamental properties. Density Functional Theory (DFT) calculations, using the PBE0 functional and the 6-31+G* basis set, were performed in an implicit medium, provided by the polarizable continuum model (PCM), to account for aqueous solvent effects.[40,41]

Monomer conformations are shown in Figure 6. Those structures were obtained after performing a conformational search

DOI: 10.1021/acs.biomac.6b01156
Biomacromolecules 2016, 17, 3659−3671

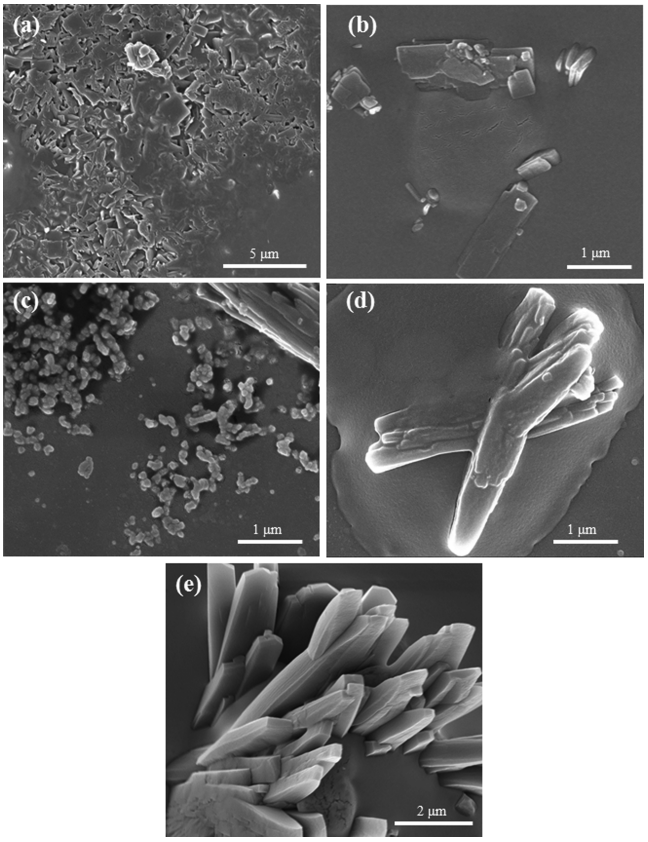

Figure 5. SEM images corresponding to telaprevir crystals after crystallization induction time experiments in the presence of 5 μg/mL predissolved polymer: (a) HPMC, (b) HPMCAS-MF, (c) CA-Sub-090, (d) PVP, (e) phosphate buffer. The shape and size of the crystal is drastically changed by the presence of polymer.

procedure and a subsequent geometry optimization on the lowest energy conformer. Along with each monomer structure, the molecular electrostatic potential (MEP) is mapped over an iso-surface of the electronic density, a region of the space enclosing a given probability of finding an electron. The MEP is expressed as a color scale where the different colors indicate the value of the potential at that point of the surface. The color coding matches those of the rainbow, with purple on one extreme, indicating positive charge accumulation, and red on the opposite end, indicating an overall negative region of the MEP. Ideally, the information provided by the MEP allows the recognition of atoms, groups, or regions of the molecule that are inclined to interact with positively charged, neutral, or negatively charged species. The MEP-mapped electronic density offers a visual indication about regions in where short (0 to ~0.2 nm) and medium range (~0.2 to ~0.5 nm) noncovalent interactions are probable, namely, electrostatics and hydrogen bonding.

Figure 6 highlights the fact that monomer conformation is highly dependent on the nature of the substituents. For instance, A1a, A2a, and A5a favor extended side chain conformations, whereas A1b, A2b, A4a, A5b, A6, and A7 prefer globular conformations. In other words, the latter monomers show a predisposition for self-interaction. Additionally, the carboxylate termination in the Adp and Sub polymers induces the chain to bend toward the cellulose ring due to potential intramolecular hydrogen bond interactions. It is also clear that, while the carboxylate termination (A5a, A5b, A6, Adp, and Sub) generates negative charge accumulation over the side chain

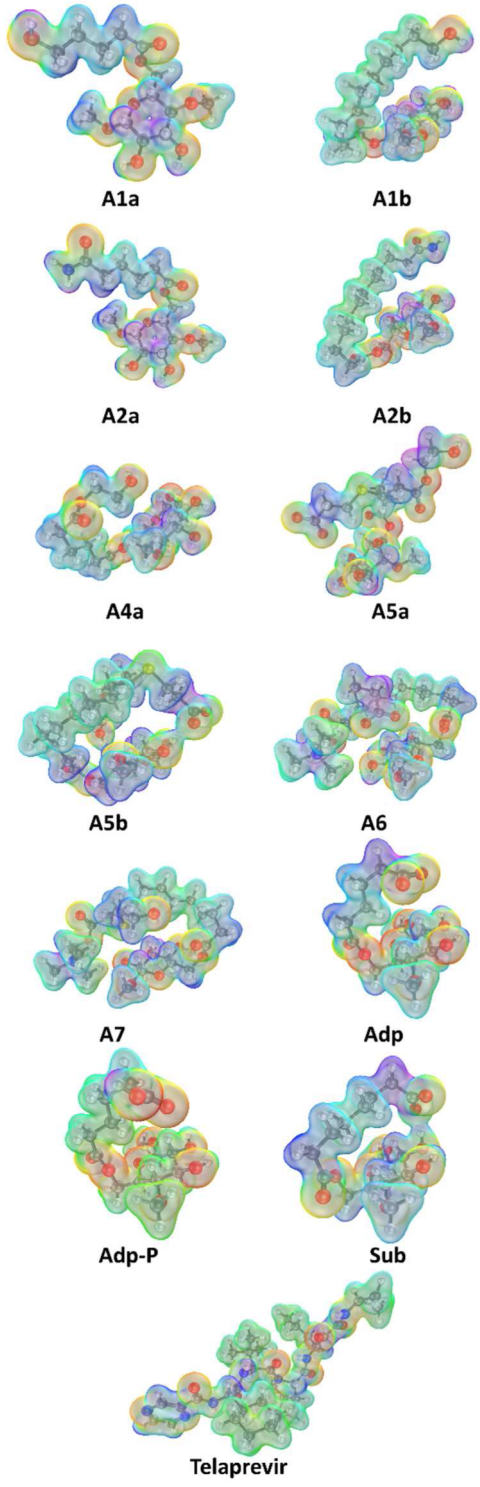

Figure 6. MEP-mapped electronic density iso-surfaces for cellulose monomers with chemically diverse substituents. The rainbow coloring represents the charge accumulation over each region of the molecule: purple indicates positive charge accumulation and red corresponds to a negative region. The illustrations provide information about tendency to establish short- and medium-range intramolecular interactions, such as electrostatic attractions or hydrogen bonding.

terminus, the alcohol (A1a and A1b) or amide termination (A2a and A2b) creates positive charge accumulation.

These quantum chemical results offer a first indication as to why A5a and A5b vary in effectiveness. A5b tends to

DOI: 10.1021/acs.biomac.6b01156
Biomacromolecules 2016, 17, 3659−3671

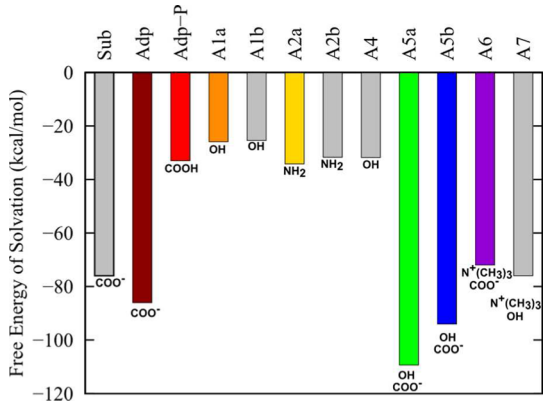

Figure 7. Free energy of solvation (kcal/mol) in PCM-modeled water for the monomeric units shown in Figures 1 and 6. Adp-P stands for protonated adipate. The terminal functional group is shown in the bottom of each bar.

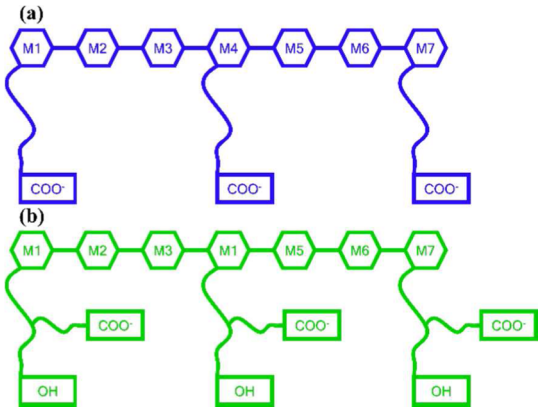

Figure 8. Schematic representation of cellulose oligomers: (a) linear side-chained and (b) branched side-chained.

self-aggregate due to its long side chain, contrary to A5a, which prefers an extended conformation. In other words, the polymer with the longer side chain (A5b) is more likely to establish attractive intramolecular interactions using both hydrophobic and hydrogen bonds, potentially restricting intermolecular interactions with drug molecules. This might also explain why A6 and A7 are ineffective, since both tend to self-aggregate.

Figure 7 presents the free energies of solvation (ΔG_{solv}) of each monomer in PCM water. The presence of charged groups, such as carboxylate and quaternary amines, contributes to more negative free energies. When comparing ionized Adp versus protonated Adp-P, their ΔG_{solv} values are drastically different. This supports the idea that sufficient amphiphilicity is only achieved when the polymer is ionized, which in turn explains why polymers with a carboxylic acid termination are only effective when ionized (e.g., neutral pH). In addition, the ΔG_{solv} of a monomer including a protonated carboxylic acid, such as Adp-P, is similar to that of a monomer containing an alcohol or an amide, which are equally ineffective. ΔG_{solv} provides significant information about the behavior of the system and may give a first indication about polymer amphiphilicity.

Molecular Dynamics Simulations. While MEP and solvation free energies of monomers provide useful information about structure−activity relationships in polymers, modeling of monomer units does not help to understand interactions among side chains in a polymer, which might be another factor determining their effectiveness. However, since quantum chemical simulations are computationally demanding for large systems, classical force field molecular dynamics (MD) was employed to explore conformations and dynamics of oligomer chains in water, to complement the information obtained from the quantum chemical calculations of monomers.

Each oligomer included seven monomers, and three of those were substituted on the R_6 group to give a degree of substitution of around 0.42, as shown in Figure 8. Representative conformations of the oligomers extracted from MD trajectories are shown in Figure 9.

A consistent color scheme for different polymers is used in Figures 7, 9, and 10. The radius of gyration, R_g, (Figure 10a) and the solvent accessible surface (SAS) area (Figure 10b) provide essential information about preferred oligomer conformations during the MD trajectory (see Materials and Methods section on detail of how R_g and SAS are computed).

We derive the following observations from Figures 9 and 10. First, polymers with long hydrocarbon side chains, A5b and A6, self-aggregate as evidenced by their lower R_g and SAS area per atom, which agrees with quantum simulations showing A5b, A6, and A7 in globular conformations, and A5a in an extended conformation. Second, similar R_g are observed for oligomers with protonated (Adp-P) and ionized (Adp) carboxylic acid and amide (A2a) groups. Third, R_g of the oligomer with the alcohol termination, A1a, is smaller than that of oligomers with amide and carboxylic acid groups. Finally, the SAS area is slightly higher in the ionized Adp than in protonated Adp-P, due to more extended side chains when the carboxylic acid group is ionized, as seen in Figure 9.

Further, Radial Distribution Functions (RDF; see Materials and Methods section for details) were computed between

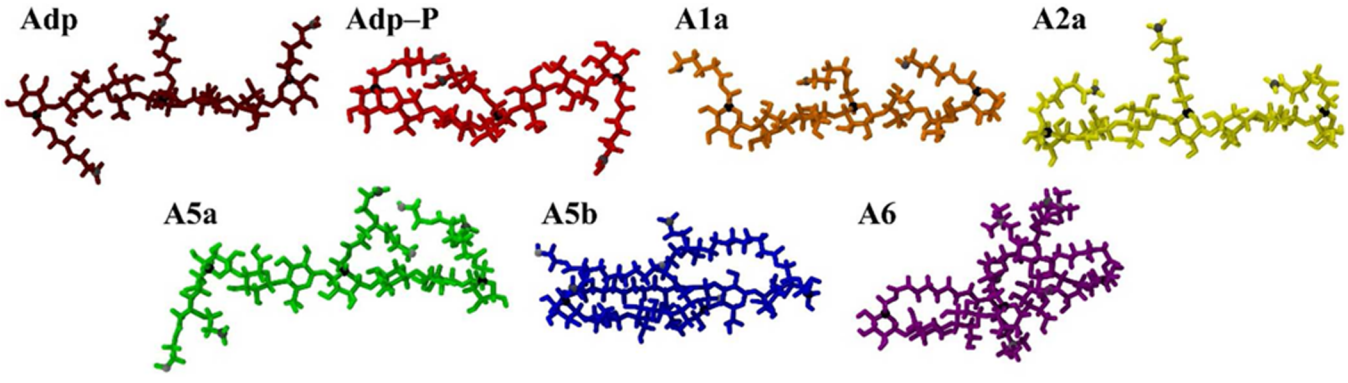

Figure 9. Representative conformations of the model oligomers extracted from the MD production trajectories.

DOI: 10.1021/acs.biomac.6b01156
Biomacromolecules 2016, 17, 3659−3671

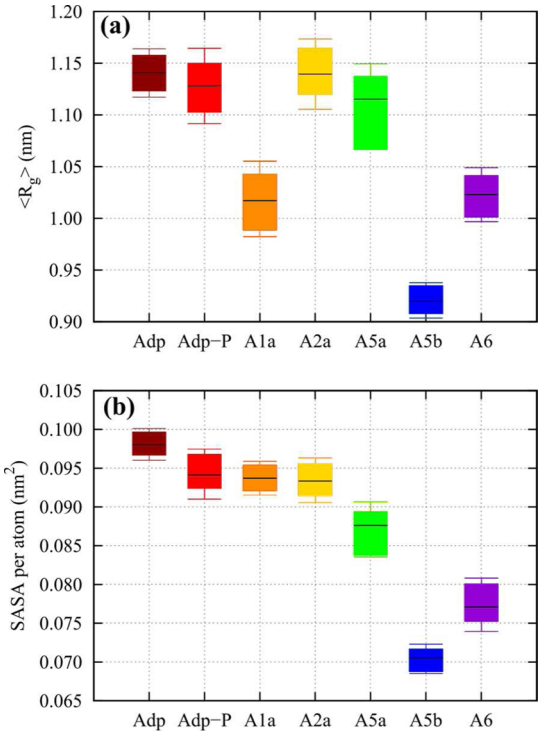

Figure 10. (a) Average radius of gyration $\langle R_g \rangle$ and (b) solvent accessible surface area per atom for a group of seven oligomers. Data processed from the production trajectories. The arithmetic mean is marked by the black horizontal line, accompanied by candlesticks, centered on the median, representing the standard deviation. The whisker bars mark the lower and higher quartiles, meaning that 50% of all measurements are contained within these bars.

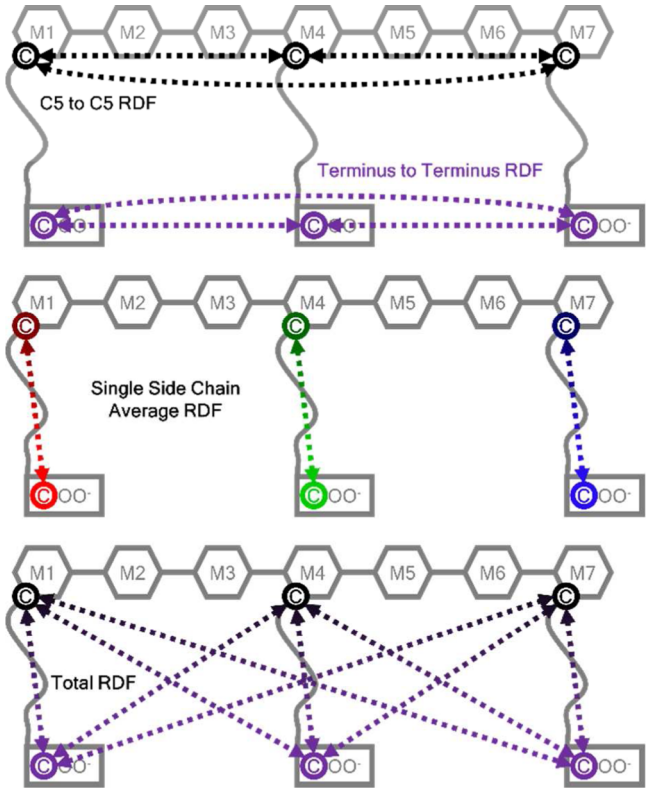

Figure 11. Schematic representation showing the atom group definitions employed to calculate RDFs. Each color represents a group. The dotted lines show sampled distances.

groups of atoms schematically shown in Figure 11. In the first case, a terminal atom of each R_6 substituent was selected as one group. The RDF between all possible pairs of these atoms is designated as the terminal-to-terminal RDF. In the second case, all carbon 5 (C5) atoms, where the substituent side chain is attached to the anhydroglucose ring, were selected as a group. The RDF between all possible pairs of C5 atoms is denoted as the C5-to-C5 RDF. In the third case, a terminal atom of each R_6 substituent and the carbon 5 (C5) were selected. Then, an average RDF was constructed with the information on the three side chains. This is designated the single side chain average RDF. In the fourth case, one group contained all three C5 atoms and the other contained all three terminal atoms, such that the RDF contains information about all side chains interacting with all C5s simultaneously. This is named a total RDF.

Figures 12 and 13 provide information about the oligomer conformation dynamics throughout the trajectory via RDFs. Figure 12a shows both the C5-to-C5 RDFs and the terminus-to-terminus RDF. The C5-to-C5 RDFs attest to the observation that the structure of the main cellulose chain is stiff and remains extended for A2a, Adp, Adp-P, and A5a, as indicated by a prominent maximum at ∼1.5 nm. In contrast, the main cellulose chain structures of A1a, A5b, and A6 are more flexible, with two broad maxima observed at ∼1.25 nm and ∼1.5 nm. The results on Figure 12 strongly correlate with those of R_g on Figure 10, suggesting that R_g primarily depends on the conformation of the main cellulose chain and that the SAS area is well correlated with the conformation of the substituent side chains.

Figure 12b presents information on the interaction between side chains in the oligomer, through the terminus-to-terminus RDFs. There is only one terminus on the A1a, A2a, Adp, and Adp-P side chains, and two termini in A5a, A5b, and A6. In the latter cases, the plot includes the RDFs between all possible terminal combinations, as labeled on the curves.

Two observations are noteworthy: first, there appears evidence of hydrogen bonding between side-chain termini in A1a, A5a, and A5b. These three show maxima at close separations between OH groups, and additionally, A5a and A5b show a narrow band at close separations between COO^- and OH groups. Interestingly, in the case of A6, there is clear evidence of repulsion between same-charge terminals, but close contacts between oppositely charged COO^- and $N^+(CH_3)_3$ groups. Second, in side chains with same-sign charges (Adp, A5b, and A6), broad RDFs provide evidence of repulsions between termini, with the notable exception of A5a, probably because the torsional freedom of the side chain is limited by its short length. Within the set of nonbranched oligomers, the only oligomer that shows evidence of repulsion between termini is Adp.

Figure 13 shows the single side chain average and the total RDFs, between C5s and terminal atoms. The RDF of Adp (COO^-) has a predominant peak at ∼0.8 nm. This peak is broadened in A1a (OH), A2a (NH_2), and Adp-P (COOH), showing a wider and noisier distribution. The RDF analysis, as well as the inspection of the trajectories, indicates that A1a, A2a, and Adp-P side chains are more dynamic and flexible than those of Adp. This is probably due to the repulsion between the partial negative charges located at the terminal carboxylate groups.

It is noteworthy that classical simulations of an oligomer of Adp show more extended conformations of the ionized side chains compared to a more globular conformation of the corresponding monomer observed in the quantum calculations.

DOI: 10.1021/acs.biomac.6b01156
Biomacromolecules 2016, 17, 3659−3671

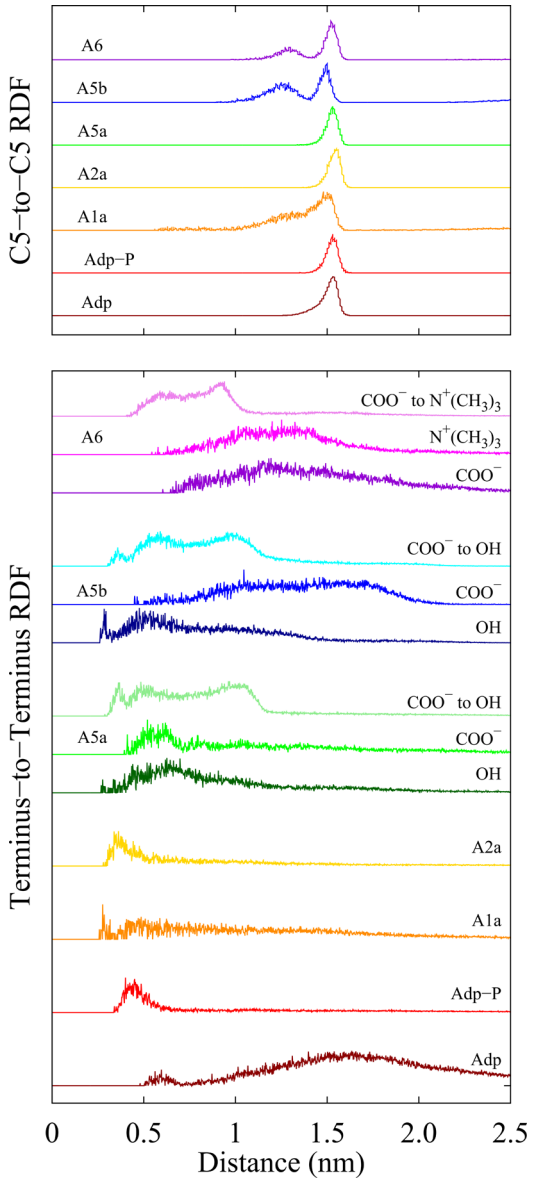

Figure 12. Radial Distribution Function (RDF) for different oligomers: (a) C5-to-C5 RDF and (b) terminus-to-terminus RDF.

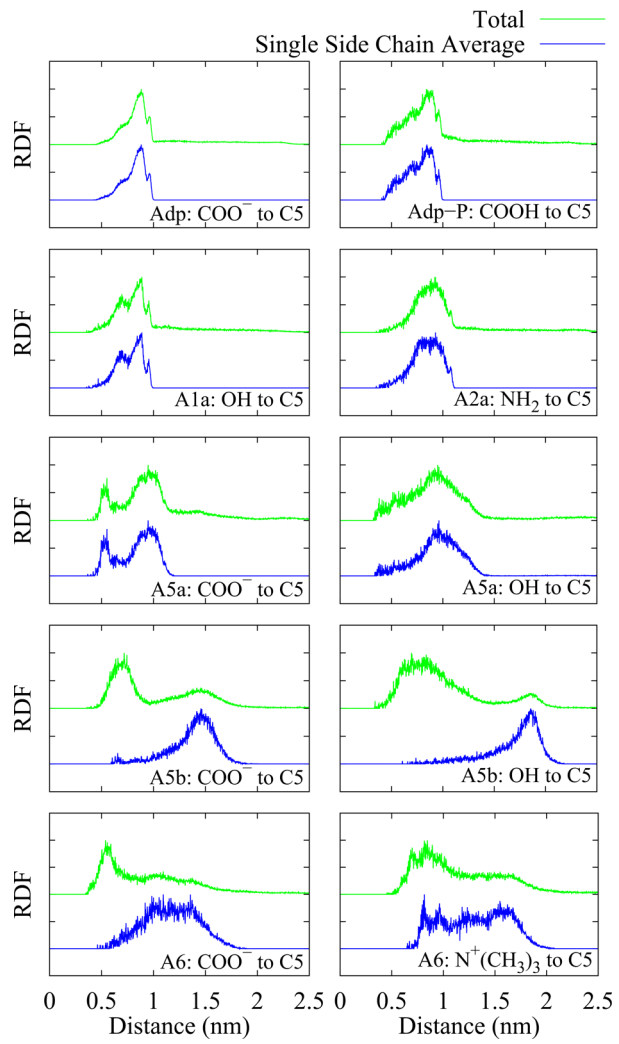

Figure 13. Radial Distribution Function (RDF) for different oligomers, showing the single side chain average RDF in blue, and the total RDF in green.

This important difference can be attributed to the effect of the charged neighbor side chains in polymer simulations. In the oligomer, the other charged side chains make it difficult for the COO^- group to bend toward the cellulose, whereas in the case of a single monomer, bending of the COO^- group to the cellulose ring is sterically unconstrained and energetically favorable.

There is a correspondence between the single side chain average (blue) and total (green) RDFs of A1a (OH), A2a (NH_2), Adp (COO^-), Adp-P (COOH), and A5a (branched with short hydrocarbon chain) oligomers, showing that the side chains prefer to extend, distancing themselves from the cellulose rings. In contrast, the single side chain average and total RDFs of A5b and A6 (branched with long hydrocarbon chains) are notably different. Inspection of the trajectories reveals that the two side chains on the extremes of A5b and A6 oligomers lean toward the center of the polymer, while the side chain on the center bends toward either side of the polymer, as is exemplified in Figure 9.

As a consequence, in A5b the C5 and COO^- are separated by ∼1.5 nm according to the single side chain average RDF, while the total C5 to COO^- RDF has a maximum at ∼0.5 nm. In other words, the COO^- groups of the side chains on the extremes are most probably found nearby the central C5, at ∼0.5 nm, whereas COO^- of the central side chain locates close to the C5s on either extreme, also at ∼0.5 nm; however, all COO^- groups are most probably found at ∼1.5 nm from their own C5.

A rather similar behavior is observed in A6. It self-aggregates, as it can be seen in Figure 9. However, A6 shows richer dynamics than A5b. Therefore, the A6 RDF shows a broader range of probable separations.

DISCUSSION

The design of new polymeric materials for amorphous dispersions is essential to address issues with the oral drug delivery of emerging poorly water-soluble therapeutics, but is currently an empirical process due to the lack of fundamental correlation between polymer structure and performance. Herein, the impact of diverse chemical substituents on the effectiveness of polymers as crystallization inhibitors has been specifically evaluated in order to better understand structure−activity relationships.

DOI: 10.1021/acs.biomac.6b01156
Biomacromolecules 2016, 17, 3659−3671

The most effective polymers included CAP-Adp-085, CA-Sub-090, CA-Adp-067, CA-Adp-056, and CA-A5a-079, which share a common chemical feature: carboxylate groups. In contrast, polymers with other terminal functional groups, such as alcohol, ether, amide, protonated carboxylic acid, and quaternary amine groups were ineffective. However, Figure 2a clearly shows that not all polymers that include carboxylic acid groups are effective crystallization inhibitors: Pectin, PAA, and EUD L100 had minimal impact on induction times. These results agree with previous reports indicating that PAA and EUD L100 are ineffective,[8,52,53] probably due to a combination of factors that include hydrophilicity, the absence of branches and bulky groups that can form favorable interactions with the drug molecules, and prevent crystallization.[8]

No correlation was found between glass transition temperature or molecular weight and polymer effectiveness. Furthermore, only a weak correlation between SP and polymer effectiveness existed across this chemically diverse polymer set, in contrast to stronger correlations within more structurally homogeneous polymer sets in previous literature reports.[8,22] Calculated SPs appear to be insufficient to accurately describe amphiphilicity across the broader range of complex polymer molecular structures.

Alternatively, quantum chemical calculations of monomers and classical simulations of oligomers provided revealing information regarding preferred structure conformation and thermodynamics of solvation. These results indicate that effective cellulose polymers should not only have carboxylate terminal groups, but these carboxylic acid groups must sufficiently enhance the hydrophilicity of the polymer to counteract the formation of intramolecular hydrophobic interactions.

Comparison of ΔG_{solv} between monomers can be used to indirectly estimate how much a group contributes to the hydrophilicity of the polymer. For instance, charged groups, such as carboxylate and quaternary amines, contribute to a more negative ΔG_{solv}; whereas monomers with a protonated carboxylic acid, alcohol, and amide groups have similar ΔG_{solv} values. According to literature reports, ΔG_{solv} values are accurate within a margin of ~5 kcal/mol,[54] which is less than the variation in ΔG_{solv} between charged and noncharged monomers. Granted that ΔG_{solv} provides important information about the chemistry of the system and that it may give a first indication about polymer amphiphilicity, there is a weak correlation between polymer effectiveness and ΔG_{solv}. On the one hand, this thermodynamic analysis may explain why polymers with carboxylic acid termini are only effective when ionized (Figure 3), while polymers with amide, alcohol and protonated carboxylic acid groups are ineffective. On the other hand, A5b ($-COO^-$), A6 ($-N^+C(CH_3)_3$ and $-COO^-$), and A7 ($-N^+C(CH_3)_3$) have more negative ΔG_{solv} than neutral monomers, due to the presence of charged groups, but they are ineffective. In other words, ΔG_{solv} in isolation is not predictive of polymer effectiveness.

The ineffectiveness of A5b, A6, and A7 can be rationalized by considering the results of both quantum chemical and classical simulations. These studies reveal that the polymers tend to self-aggregate, implying that the hydrophilicity conferred by the presence of charged groups is insufficient to overcome the intramolecular hydrophobic interactions between the hydrocarbon side chains and the cellulose rings. Consequently, these polymers are not truly amphiphilic, which appears to be an important requirement for effective materials. Thus, this study suggests that the right balance between key substituent groups and the hydrocarbon side chain length needs to be met in order to create effective polymers. For polymers to be effective, it is essential that they possess both sufficient hydrophobic regions to drive interactions with the drug and adequate hydrophilicity to promote solvation in an aqueous environment.

Previous studies have highlighted the importance of polymer conformation for crystallization inhibition, as well as the role of ionization in impacting polymer conformation. AFM experiments have previously shown that the conformation of the polymer on a crystal surface is a key determinant of effectiveness at inhibiting crystal growth.[23,24] For instance, HPMCAS, a commonly used polymer with carboxylic acid groups, was effective at inhibiting crystal growth at neutral pH and ineffective at low pH.[23] When analyzing the surface topography by AFM, globules of polymer were observed at low pH, while extended polymer chains were present at neutral pH.[23] These observations are in good agreement with MD simulations in chitosan nanohydrogels, showing that R_g depends on the percentage of protonated monomers, with large R_g values found in charged chains and small R_g observed in neutral chains.[55] Our findings also broadly agree with Lennard-Jones MD simulations by Anwar et al., who suggested that effective crystallization inhibitors require the right balance between the affinity of the inhibitor for the crystallizing solute relative to self-affinity and solvent affinity.[26] Our observations are also in accordance with MD simulations by Mackenzie et al., showing that an optimal degree of polymer hydrophobicity is required to have a good encapsulation efficiency in drug-polymer nanoparticles.[30]

Our results support the supposition that the solvated polymer conformation plays a major role in its effectiveness as a crystallization inhibitor. The simulations provide critical insight, helping to explain why structurally similar polymers vary in effectiveness. For instance, for the chemically similar polymers A5a and A5b, the former polymer is effective because it has a more extended conformation while A5b is not effective because it tends to self-aggregate. Without the information provided from molecular modeling, it was difficult to explain why these two polymers differed so drastically in terms of impact on telaprevir crystallization.

This study highlights the importance of combining experimental results and computational modeling when designing new polymeric materials for the delivery of poorly water-soluble drugs. The combined quantum and classical computational approaches support experimental findings and reveal the ways in which changes in the chemical structure alter the monomer and oligomer conformations and, by inference, the availability of the polymer to effectively interact with drug molecules to disrupt their self-association into an ordered crystal. In other words, it is difficult to make predictions based on evaluation of the monomer chemical structure, because it is unclear how conformation and chemistry will be changed upon oligomerization and solvation. We are optimistic that the combination of experiments with molecular modeling will assist in achieving a molecular understanding of how changes in polymer molecular structure can be extrapolated to differences in effectiveness at disrupting crystallization.

CONCLUSION

This study combined experimental results and computational modeling to explain differences in polymer effectiveness at inhibiting drug crystallization from solution. After analyzing a group of newly synthesized chemically diverse cellulose-based polymers, including carboxylic acids, esters, ethers, alcohols, amides, amines, and sulfides groups, it was concluded that the

DOI: 10.1021/acs.biomac.6b01156
Biomacromolecules 2016, 17, 3659−3671

effective polymers contained carboxylate groups in combination with an optimal hydrocarbon chain length. As made clear by quantum chemical calculations, the effectiveness of carboxylate groups was attributed to a more favorable solvation free energy, in comparison to noncharged groups. Moreover, molecular dynamics simulations of oligomers showed that polymers with long hydrocarbon chains tend to self-aggregate exhibiting shorter radii of gyration and solvent accessible surface areas per atom. The knowledge gained from this study will inform the next steps in polymer design, whereby materials with ionized groups that are not hindered by intramolecular interactions will be synthesized. This will be attained by finding the right balance between carboxylate groups and hydrophobic side chains, yielding promising new materials for amorphous dispersions. The combined experimental-computational approach to optimize crystallization inhibition properties of cellulose polymers is readily extendable for the rational design of polymers for other drug delivery applications.

■ ASSOCIATED CONTENT

Supporting Information

The Supporting Information is available free of charge on the ACS Publications website at DOI: 10.1021/acs.biomac.6b01156.

Details about the physicochemical properties and calculated solubility parameters of the polymers, as well as the methodology used for their characterization (PDF).

■ AUTHOR INFORMATION

Corresponding Author

*E-mail: lstaylor@purdue.edu. Fax: +1 (765) 494-6545. Tel.: +1 (765) 714-2808.

Author Contributions

The manuscript was written through contributions of all authors. All authors have given approval to the final version of the manuscript.

Notes

The authors declare no competing financial interest.

■ ACKNOWLEDGMENTS

We thank the National Science Foundation for funding this work through Award Numbers DMR-1308276, DMR-1309218, and CHE-1465154. This research was supported in part by a Graduate Student Fellowship Award from the American Association of Pharmaceutical Scientists to L.M. We are grateful to Dr. Christopher J. Gilpin and Chia-Ping Huang from the Life Sciences Microscopy Facility for the helpful discussions about the SEM analysis. This research was supported in part through computational resources provided by Information Technology at Purdue University.

■ REFERENCES

(1) Thayer, A. M. Finding solutions. *Chem. Eng. News* **2010**, *88* (22), 13−18.

(2) Newman, A.; Knipp, G.; Zografi, G. Assessing the performance of amorphous solid dispersions. *J. Pharm. Sci.* **2012**, *101* (4), 1355−1377.

(3) Williams, H. D.; Trevaskis, N. L.; Charman, S. A.; Shanker, R. M.; Charman, W. N.; Pouton, C. W.; Porter, C. J. Strategies to address low drug solubility in discovery and development. *Pharmacol. Rev.* **2013**, *65* (1), 315−499.

(4) Baghel, S.; Cathcart, H.; O'Reilly, N. J. Polymeric Amorphous Solid Dispersions: A Review of Amorphization, Crystallization, Stabilization, Solid-State Characterization, and Aqueous Solubilization of Biopharmaceutical Classification System Class II Drugs. *J. Pharm. Sci.* **2016**, *105* (9), 2527−44.

(5) Otsuka, M.; Kaneniwa, N. A Kinetic Study of the Crystallization Process of Noncrystalline Indomethacin under Isothermal Conditions. *Chem. Pharm. Bull.* **1988**, *36* (10), 4026−4032.

(6) Broman, E.; Khoo, C.; Taylor, L. S. A comparison of alternative polymer excipients and processing methods for making solid dispersions of a poorly water soluble drug. *Int. J. Pharm.* **2001**, *222* (1), 139−151.

(7) Vandecruys, R.; Peeters, J.; Verreck, G.; Brewster, M. E. Use of a screening method to determine excipients which optimize the extent and stability of supersaturated drug solutions and application of this system to solid formulation design. *Int. J. Pharm.* **2007**, *342* (1−2), 168−175.

(8) Ilevbare, G. A.; Liu, H.; Edgar, K. J.; Taylor, L. S. Maintaining Supersaturation in Aqueous Drug Solutions: Impact of Different Polymers on Induction Times. *Cryst. Growth Des.* **2013**, *13* (2), 740−751.

(9) Ting, J. M.; Navale, T. S.; Bates, F. S.; Reineke, T. M. Design of Tunable Multicomponent Polymers as Modular Vehicles To Solubilize Highly Lipophilic Drugs. *Macromolecules* **2014**, *47* (19), 6554−6565.

(10) Liu, H.; Ilevbare, G. A.; Cherniawski, B. P.; Ritchie, E. T.; Taylor, L. S.; Edgar, K. J. Synthesis and structure−property evaluation of cellulose ω-carboxyesters for amorphous solid dispersions. *Carbohydr. Polym.* **2014**, *100*, 116−125.

(11) Ting, J. M.; Navale, T. S.; Jones, S. D.; Bates, F. S.; Reineke, T. M. Deconstructing HPMCAS: Excipient Design to Tailor Polymer−Drug Interactions for Oral Drug Delivery. *ACS Biomater. Sci. Eng.* **2015**, *1* (10), 978−990.

(12) Liu, H.; Taylor, L. S.; Edgar, K. J. The role of polymers in oral bioavailability enhancement; a review. *Polymer* **2015**, *77*, 399−415.

(13) Yin, L.; Hillmyer, M. A. Preparation and Performance of Hydroxypropyl Methylcellulose Esters of Substituted Succinates for in Vitro Supersaturation of a Crystalline Hydrophobic Drug. *Mol. Pharmaceutics* **2014**, *11* (1), 175−185.

(14) Meng, X.; Matson, J. B.; Edgar, K. J. Olefin cross-metathesis, a mild, modular approach to functionalized cellulose esters. *Polym. Chem.* **2014**, *5* (24), 7021−7033.

(15) Meng, X.; Matson, J. B.; Edgar, K. J. Olefin Cross-Metathesis as a Source of Polysaccharide Derivatives: Cellulose ω-Carboxyalkanoates. *Biomacromolecules* **2014**, *15* (1), 177−187.

(16) Meng, X.; Edgar, K. J. Synthesis of amide-functionalized cellulose esters by olefin cross-metathesis. *Carbohydr. Polym.* **2015**, *132*, 565−573.

(17) Meng, X.; York, E. A.; Liu, S.; Edgar, K. J. Hydroboration−oxidation: A chemoselective route to cellulose ω-hydroxyalkanoate esters. *Carbohydr. Polym.* **2015**, *133*, 262−269.

(18) Dong, Y.; Edgar, K. J. Imparting functional variety to cellulose ethers via olefin cross-metathesis. *Polym. Chem.* **2015**, *6* (20), 3816−3827.

(19) Dong, Y.; Mosquera-Giraldo, L. I.; Taylor, L. S.; Edgar, K. J. Amphiphilic Cellulose Ethers Designed for Amorphous Solid Dispersion via Olefin Cross-Metathesis. *Biomacromolecules* **2016**, *17* (2), 454−465.

(20) Meng, X.; Roy Choudhury, S.; Edgar, K. J. Multifunctional cellulose esters by olefin cross-metathesis and thiol-Michael addition. *Polym. Chem.* **2016**, *7* (23), 3848−3856.

(21) Ilevbare, G. A.; Liu, H.; Edgar, K. J.; Taylor, L. S. Inhibition of solution crystal growth of ritonavir by cellulose polymers - factors influencing polymer effectiveness. *CrystEngComm* **2012**, *14* (20), 6503−6514.

(22) Ilevbare, G. A.; Liu, H.; Edgar, K. J.; Taylor, L. S. Impact of Polymers on Crystal Growth Rate of Structurally Diverse Compounds from Aqueous Solution. *Mol. Pharmaceutics* **2013**, *10* (6), 2381−2393.

(23) Schram, C. J.; Beaudoin, S. P.; Taylor, L. S. Impact of Polymer Conformation on the Crystal Growth Inhibition of a Poorly Water-Soluble Drug in Aqueous Solution. *Langmuir* **2015**, *31* (1), 171−179.

(24) Schram, C. J.; Taylor, L. S.; Beaudoin, S. P. Influence of Polymers on the Crystal Growth Rate of Felodipine: Correlating

DOI: 10.1021/acs.biomac.6b01156
Biomacromolecules 2016, 17, 3659−3671

Adsorbed Polymer Surface Coverage to Solution Crystal Growth Inhibition. *Langmuir* **2015**, *31* (41), 11279−11287.
(25) Fedors, R. F. A method for estimating both the solubility parameters and molar volumes of liquids. *Polym. Eng. Sci.* **1974**, *14* (2), 147−154.
(26) Anwar, J.; Boateng, P. K.; Tamaki, R.; Odedra, S. Mode of Action and Design Rules for Additives That Modulate Crystal Nucleation. *Angew. Chem., Int. Ed.* **2009**, *48* (9), 1596−1600.
(27) Jha, P. K.; Larson, R. G. Assessing the Efficiency of Polymeric Excipients by Atomistic Molecular Dynamics Simulations. *Mol. Pharmaceutics* **2014**, *11* (5), 1676−1686.
(28) Gao, Y.; Olsen, K. W. Drug−Polymer Interactions at Water−Crystal Interfaces and Implications for Crystallization Inhibition: Molecular Dynamics Simulations of Amphiphilic Block Copolymer Interactions with Tolazamide Crystals. *J. Pharm. Sci.* **2015**, *104* (7), 2132−2141.
(29) Ahmad, S.; Johnston, B. F.; Mackay, S. P.; Schatzlein, A. G.; Gellert, P.; Sengupta, D.; Uchegbu, I. F. In silico modelling of drug−polymer interactions for pharmaceutical formulations. *J. R. Soc., Interface* **2010**, *7* (Suppl 4), S423−S433.
(30) Mackenzie, R.; Booth, J.; Alexander, C.; Garnett, M. C.; Laughton, C. A. Multiscale Modeling of Drug−Polymer Nanoparticle Assembly Identifies Parameters Influencing Drug Encapsulation Efficiency. *J. Chem. Theory Comput.* **2015**, *11* (6), 2705−2713.
(31) Maniruzzaman, M.; Pang, J.; Morgan, D. J.; Douroumis, D. Molecular Modeling as a Predictive Tool for the Development of Solid Dispersions. *Mol. Pharmaceutics* **2015**, *12* (4), 1040−1049.
(32) Maniruzzaman, M.; Snowden, M. J.; Bradely, M. S.; Douroumis, D. Studies of intermolecular interactions in solid dispersions using advanced surface chemical analysis. *RSC Adv.* **2015**, *5* (91), 74212−74219.
(33) Kwong, A. D.; Kauffman, R. S.; Hurter, P.; Mueller, P. Discovery and development of telaprevir: an NS3−4A protease inhibitor for treating genotype 1 chronic hepatitis C virus. *Nat. Biotechnol.* **2011**, *29* (11), 993−1003.
(34) Meng, X.; Edgar, K. J. Click" reactions in polysaccharide modification. *Prog. Polym. Sci.* **2016**, *53*, 52.
(35) Babcock, W. C.; Friesen, D. T.; Lyon, D. K.; Miller, W. K.; Smithey, D. T. Pharmaceutical compositions with enhanced performance. WO2005115330 A2, Dec 8, 2005.
(36) Mosquera-Giraldo, L. I.; Taylor, L. S. Glass−Liquid Phase Separation in Highly Supersaturated Aqueous Solutions of Telaprevir. *Mol. Pharmaceutics* **2015**, *12* (2), 496−503.
(37) Almeida e Sousa, L.; Reutzel-Edens, S. M.; Stephenson, G. A.; Taylor, L. S. Assessment of the Amorphous "Solubility" of a Group of Diverse Drugs Using New Experimental and Theoretical Approaches. *Mol. Pharmaceutics* **2015**, *12* (2), 484−495.
(38) Ernzerhof, M.; Scuseria, G. E. Assessment of the Perdew−Burke−Ernzerhof exchange-correlation functional. *J. Chem. Phys.* **1999**, *110* (11), 5029−5036.
(39) Adamo, C.; Barone, V. Toward reliable density functional methods without adjustable parameters: The PBE0 model. *J. Chem. Phys.* **1999**, *110* (13), 6158−6170.
(40) Miertuš, S.; Scrocco, E.; Tomasi, J. Electrostatic interaction of a solute with a continuum. A direct utilizaion of AB initio molecular potentials for the prevision of solvent effects. *Chem. Phys.* **1981**, *55* (1), 117−129.
(41) Mennucci, B. Polarizable continuum model. *Wiley Interdisciplinary Reviews: Computational Molecular Science* **2012**, *2* (3), 386−404.
(42) Gilbert, A. IQmol molecular viewer. 2012; http://iqmol.org/.
(43) Froimowitz, M. HyperChem: a software package for computational chemistry and molecular modeling. *Biotechniques* **1993**, *14* (6), 1010−1013.
(44) Gelbrich, T.; Kahlenberg, V.; Langes, C.; Griesser, U. J. Telaprevir: helical chains based on three-point hydrogen-bond connectionsCAS number: 402957−28−2. *Acta Crystallogr., Sect. C: Cryst. Struct. Commun.* **2013**, *69* (2), 179−182.
(45) Shao, Y.; Gan, Z.; Epifanovsky, E.; Gilbert, A. T. B.; Wormit, M.; Kussmann, J.; Lange, A. W.; Behn, A.; Deng, J.; Feng, X.; Ghosh, D.; Goldey, M.; Horn, P. R.; Jacobson, L. D.; Kaliman, I.; Khaliullin, R. Z.; Kuś, T.; Landau, A.; Liu, J.; Proynov, E. I.; Rhee, Y. M.; Richard, R. M.; Rohrdanz, M. A.; Steele, R. P.; Sundstrom, E. J.; Woodcock, H. L.; Zimmerman, P. M.; Zuev, D.; Albrecht, B.; Alguire, E.; Austin, B.; Beran, G. J. O.; Bernard, Y. A.; Berquist, E.; Brandhorst, K.; Bravaya, K. B.; Brown, S. T.; Casanova, D.; Chang, C.-M.; Chen, Y.; Chien, S. H.; Closser, K. D.; Crittenden, D. L.; Diedenhofen, M.; DiStasio, R. A.; Do, H.; Dutoi, A. D.; Edgar, R. G.; Fatehi, S.; Fusti-Molnar, L.; Ghysels, A.; Golubeva-Zadorozhnaya, A.; Gomes, J.; Hanson-Heine, M. W. D.; Harbach, P. H. P.; Hauser, A. W.; Hohenstein, E. G.; Holden, Z. C.; Jagau, T.-C.; Ji, H.; Kaduk, B.; Khistyaev, K.; Kim, J.; Kim, J.; King, R. A.; Klunzinger, P.; Kosenkov, D.; Kowalczyk, T.; Krauter, C. M.; Lao, K. U.; Laurent, A. D.; Lawler, K. V.; Levchenko, S. V.; Lin, C. Y.; Liu, F.; Livshits, E.; Lochan, R. C.; Luenser, A.; Manohar, P.; Manzer, S. F.; Mao, S.-P.; Mardirossian, N.; Marenich, A. V.; Maurer, S. A.; Mayhall, N. J.; Neuscamman, E.; Oana, C. M.; Olivares-Amaya, R.; O'Neill, D. P.; Parkhill, J. A.; Perrine, T. M.; Peverati, R.; Prociuk, A.; Rehn, D. R.; Rosta, E.; Russ, N. J.; Sharada, S. M.; Sharma, S.; Small, D. W.; Sodt, A.; Stein, T.; Stück, D.; Su, Y.-C.; Thom, A. J. W.; Tsuchimochi, T.; Vanovschi, V.; Vogt, L.; Vydrov, O.; Wang, T.; Watson, M. A.; Wenzel, J.; White, A.; Williams, C. F.; Yang, J.; Yeganeh, S.; Yost, S. R.; You, Z.-Q.; Zhang, I. Y.; Zhang, X.; Zhao, Y.; Brooks, B. R.; Chan, G. K. L.; Chipman, D. M.; Cramer, C. J.; Goddard, W. A.; Gordon, M. S.; Hehre, W. J.; Klamt, A.; Schaefer, H. F.; Schmidt, M. W.; Sherrill, C. D.; Truhlar, D. G.; Warshel, A.; Xu, X.; Aspuru-Guzik, A.; Baer, R.; Bell, A. T.; Besley, N. A.; Chai, J.-D.; Dreuw, A.; Dunietz, B. D.; Furlani, T. R.; Gwaltney, S. R.; Hsu, C.-P.; Jung, Y.; Kong, J.; Lambrecht, D. S.; Liang, W.; Ochsenfeld, C.; Rassolov, V. A.; Slipchenko, L. V.; Subotnik, J. E.; Van Voorhis, T.; Herbert, J. M.; Krylov, A. I.; Gill, P. M. W.; Head-Gordon, M. Advances in molecular quantum chemistry contained in the Q-Chem. 4 program package. *Mol. Phys.* **2015**, *113* (2), 184−215.
(46) Van Der Spoel, D.; Lindahl, E.; Hess, B.; Groenhof, G.; Mark, A. E.; Berendsen, H. J. C. Gromacs: Fast, Flexible, and Free. *J. Comput. Chem.* **2005**, *26*, 1701−1718.
(47) Hess, B.; Kutzner, C.; van der Spoel, D.; Lindahl, E. GROMACS 4: Algorithms for Highly Efficient, Load-Balanced, and Scalable Molecular Simulation. *J. Chem. Theory Comput.* **2008**, *4* (3), 435−447.
(48) Brooks, B. R.; Bruccoleri, R. E.; Olafson, B. D.; States, D. J.; Swaminathan, S.; Karplus, M. CHARMM: A program for macromolecular energy, minimization, and dynamics calculations. *J. Comput. Chem.* **1983**, *4* (2), 187−217.
(49) MacKerell, A. D.; Banavali, N.; Foloppe, N. Development and current status of the CHARMM force field for nucleic acids. *Biopolymers* **2000**, *56* (4), 257−265.
(50) Zoete, V.; Cuendet, M. A.; Grosdidier, A.; Michielin, O. SwissParam: A fast force field generation tool for small organic molecules. *J. Comput. Chem.* **2011**, *32* (11), 2359−2368.
(51) Essmann, U.; Perera, L.; Berkowitz, M. L.; Darden, T.; Lee, H.; Pedersen, L. G. A smooth particle mesh Ewald method. *J. Chem. Phys.* **1995**, *103* (19), 8577−8593.
(52) Ozaki, S.; Kushida, I.; Yamashita, T.; Hasebe, T.; Shirai, O.; Kano, K. Inhibition of crystal nucleation and growth by water-soluble polymers and its impact on the supersaturation profiles of amorphous drugs. *J. Pharm. Sci.* **2013**, *102* (7), 2273−2281.
(53) Xie, T.; Taylor, L. S. Improved Release of Celecoxib from High Drug Loading Amorphous Solid Dispersions Formulated with Polyacrylic Acid and Cellulose Derivatives. *Mol. Pharmaceutics* **2016**, *13* (3), 873−884.
(54) Takano, Y.; Houk, K. N. Benchmarking the Conductor-like Polarizable Continuum Model (CPCM) for Aqueous Solvation Free Energies of Neutral and Ionic Organic Molecules. *J. Chem. Theory Comput.* **2005**, *1* (1), 70−77.
(55) Borca, C. H.; Arango, C. A. Molecular Dynamics of a Water-Absorbent Nanoscale Material Based on Chitosan. *J. Phys. Chem. B* **2016**, *120* (15), 3754−64.

DOI: 10.1021/acs.biomac.6b01156
Biomacromolecules 2016, 17, 3659−3671